International Journal of Nanoelectronics and Materials
Volume 16 (Special Issue) December 2023 [183-193]

Numerical Simulation of Lead-Free Tin and Germanium Based All Perovskite Tandem Solar Cell

Rae-Ann Lim Jia En[1,2], Ayu Wazira Azhari[1,2,*], Dewi Suriyani Che Halin[3,4], Suhaila Sepeai[5] and Norasikin Ahmad Ludin[5]

[1]Faculty of Civil Engineering and Technology, Universiti Malaysia Perlis, 02600, Jalan Kangar-Arau, Perlis Malaysia
[2]Center of Excellence for Water Research and Environmental Sustainability Growth (WAREG), Universiti Malaysia Perlis, 02600, Jalan Kangar-Arau, Perlis Malaysia
[3]Faculty of Chemical Engineering and Technology, Universiti Malaysia Perlis, 02600, Jalan Kangar-Arau, Perlis Malaysia
[4]Center of Excellence for Geopolymer & Green Technology (CEGeoGTech), Universiti Malaysia Perlis, (UniMAP), 02600 Jalan Kangar-Arau, Perlis, Malaysia
[5]Solar Energy Research Institute (SERI), Universiti Kebangsaan Malaysia (UKM), Bangi, Selangor, Malaysia

ABSTRACT

The ability to customize the materials bandgaps makes perovskite solar cells a promising candidate for hybrid-tandem applications. This allows them to effectively utilize parts of the solar spectrum that silicon-based solar cells cannot efficiently capture, resulting in higher absorption coefficients. However, there is a lack of research on lead-free all-perovskite tandem solar cells, and secondary data on materials is limited. One of the main challenges in previous studies is the high cost and solid structure of traditional silicon-based solar cells, which require significant storage space. Additionally, lead-based perovskite solar cells pose environmental concerns due to their water solubility and potential harmful effects upon consumption. To address these issues, thin-film perovskite solar cells with liquid solvents are employed in the solar cell design. Lead is replaced with germanium and tin-based perovskites, which exhibit comparable photovoltaic performance to silicon. In the present work, the OghmaNano simulation tool was utilized to conduct numerical simulation of the perovskite design. The perovskite solar cell layers were structured as follows: FTO/ZnO/$MAGeI_3$/Spiro-OMeTAD/$FAMASnGeI_3$/Cu_2O/Au. The variables considered included optimum layer thicknesses and bandgaps, as well as the most suitable materials for the ETL and HTL, aiming to obtain the highest efficiency. Based on the simulation results, the proposed perovskite structure shows remarkable photovoltaic parameters. The Voc was measured at 0.84 V Jsc of 16.1 mA/cm², FF of 0.825, and PCE that reached 11.12%. This project contributes to future research on materials for the ETL and HTL of lead-free, tin and germanium based APTSCs.

Keywords: All perovskite tandem solar cell, lead-free perovskite, numerical simulation, OghmaNano, tin germanium

1. INTRODUCTION

Solar is a clean, green, and renewable energy source that brings forth multiple advantages to future generations and the environment in the long run. Solar energy is produced by converting sunlight into electricity in photovoltaic energy conversion. The solar cells are typically used to absorb photons emitted by the sun [1]. The solar cells can be categorized into four main classes or generations known as the first generation, second generations, third generations and fourth generations solar cells [2]. The term third-generation solar cells refer to a wide range of emerging photovoltaic technologies that are designed to overcome the limitations of traditional first-

* Corresponding authors: ayuwazira@unimap.edu.my

generation and second-generation solar cells. These newer technologies are still in the research and development stage and have not yet been widely commercialized [3].

Commonly studied third-generation solar cells include organic photovoltaics (OPV), dye-sensitized solar cells (DSSC), quantum dot solar cells, multi-junction solar cells and perovskite solar cells (PSCs). Amongst these, PSCs have gain interest due to their high absorption coefficient, long carrier diffusion, bipolar charge mobility, low exciton binding energy, and tunable bandgap [4]. However, concerns about lead toxicity have led to the exploration of various method to either reducing the leakage of lead and/or partial or full substitution of lead with other materials [5]. In lead-free halide PSCs, lead is substituted with either germanium (Ge), antimony (Sb), tin (Sn), bismuth (Bi), and indium (In). These alternative materials possess similar perovskite properties and offer higher charge carrier mobilities, better absorption coefficients, and narrower optical bandgaps compared to lead- based PSCs [6]. Among these, Sn and Ge are the most studied substitute materials for lead owing to the similarity in properties [7]. To date, the highest efficiency for a single junction tin-based PSCs was obtained by Jiang *et al*. using a triple reactant strategy which leads to an efficiency of 14.6% [8].

Recently, there has been a shift of interest in alternative PSCs design driven by the need to address the rise in the needs for renewable energy sources besides overcoming the limitations of existing solar technologies. This includes the move from single junction to tandem structures due to their potential for higher efficiency, tuneable bandgaps and ease of fabrication [9]. Single-junction PSCs face limitations in performance due to several drawbacks. They are unable to absorb the full spectrum of incident light and can only convert a fraction of sunlight input into useful output. This is because excess energy from high-energy photons is thermalized, while low-energy photons pass through the cells without being absorbed. Tandem PSCs, on the other hand, are multi-junction solar cells that utilize customizable absorption materials. The goal of tandem PSCs is to outperform single-junction Shockley-Queisser solar cells [10]. By stacking two absorbers on top of each other, tandem PSCs can respond to and absorb a wider range of the solar spectrum, potentially increasing its efficiency. Additionally, wider bandgap photo absorbers in tandem PSCs structures generate higher voltages, resulting in lower thermalization losses compared to single-junction PSCs that absorb the same quantity of photons [11]. As a result, tandem PSCs achieve higher power conversion efficiencies.

Among the first work on all perovskite tandem based PSCs was conducted by Jiang *et al*. prepared by an orthogonal solvent processing method showing an efficiency of about 7% [12]. In 2019, Palmstrom *et al*. produced a flexible and rigid all perovskite tandem solar cells (APTSCs) with the efficiency of 21.3% and 23.1% respectively by employing a nucleation layer and bandgap tuning of the A-site cations [13]. In the same year, Lin *et al*. demonstrated a higher efficiency of about 24.8% for a monolithic all perovskite tandem cells by reducing the Sn vacancies in mixed Pb-Sn perovskite [14]. To date, among the highest results was obtain by Lin *et al*. on 3D/3D bilayer Pb-Sn tandem PSCs with a certified efficiency of 28% [15]. The high efficiency of these tandem perovskite layer is mainly attributed to the Pb content in all the perovskite absorber layer.

However, very little work has been done on the lead free APTSCs. A simulation study by Madan *et al*., on low Pb content APTSCs based on $Cs_2AgBi_{0.75}Sb_{0.25}Br_6$ and $FACsPb_{0.5}Sn_{0.5}I_3$ depicted an efficiency of 17.3% [16]. It is believed that the small amount of Pb leads to the low efficiency of the simulated cells. Based on a previous simulation work by Singh *et al*., it was demonstrated that a lead-free tin based tandem PSCs design was able to achieve an efficiency of 26.72% by reducing the defect density to be as low as possible [17]. Another study by Abdelaziz *et al*., focusing on the monolithic lead-free all PSCs with $MASnI_3$ and $MASnIBr_2$ was able to achieve an efficiency of 15.66% [18]. Thus far, the highest simulated results on lead free all perovskite tandem cells were presented by Duha & Borunda by optimizing the thickness, electron affinity and capture cross section of the perovskite absorber layer [19].

The present study aims to investigate the effect of perovskite absorber thickness on the lead-free tin and germanium based all-perovskite tandem solar cells (APTSCs) through numerical simulations. In addition, different electron transport and hole transport layer materials is also being studied to further improve the efficiency of the overall perovskite structure. This simulation study, conducted using OghmaNano, is significant as it may contribute to future research on the selection of materials for both the electron transport layer and hole transport layer in tin and germanium-based all-perovskite tandem solar cells. The data collected from this project may also be useful for future laboratory work. The project aims to determine the optimal layer thicknesses and bandgaps of germanium and tin germanium-perovskites, as well as compare the power conversion efficiency (PCE) of different electron transport layer and hole transport layer materials.

2. METHODOLOGY

2.1 Device Structure

Device simulation provides an alternative way to improve the properties of a PCSs by optimization of its various parameters. The model uses Poisson's equation and carrier continuity equations to analyze the charge carrier transport electrons by solving the electrons, drift-diffusion holes and electrostatic potential. Recombination and carrier trapping are expressed using Shockley-Read-Hall formalism, and trap state distribution can be flexibly specified. Figure 1 shows the proposed APTSCs structure, which includes front and back contact layers, active perovskite layers and electron and hole transport layers.

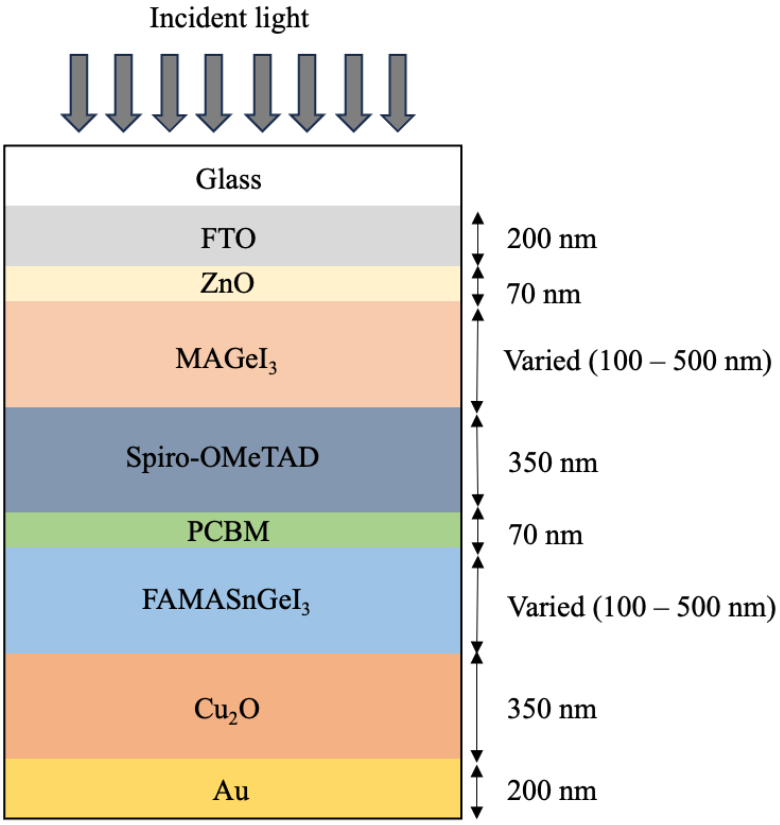

Figure 1. Design structure of the proposed APTSC.

2.2 Thickness and Bandgap Variation of Perovskite Layer

The perovskite layer thicknesses were optimized through simulation studies to give the best performance solar cell device. The thicknesses of both top wide bandgap (WBG) (Ge) and bottom narrow bandgap (NBG) (SnGe) perovskite were varied from 100 nm to 500 nm, while other layers were kept constant, as shown in Figure 1. The variation of bandgap for perovskite layers is usually ranged between 0.9 to 1.7 eV [20]. The combination of $FAMASnGeI_3$ (NBG) with 1.4 eV and $MAGeI_3$ (WBG) with 1.9 eV yielded power conversion efficiency of 26.72% [21]. Hence, the bandgap of the NBG-perovskite was varied from 1.0 eV to 1.4 eV, whereas the WBG-perovskite was varied from 1.5 eV to 2.0 eV. While NBG-perovskite bandgap is manipulated, others were kept constant. Similar steps were repeated for WBG-perovskite.

2.3 ETL and HTL Material Scan

The optimization of electron transport layer (ETL) was carried out based on built-in voltage, Vbi, analysis correlating open-circuit voltage, (Voc) across perovskite layer [17]. The minimum conduction band of the hole transport layer (HTL) must be lower than that of the perovskite layer to ensure an efficient electron transport [22]. Different ETL and HTL materials were manipulated to determine the most suitable combination that produces the best performing lead-free Ge/SnGe-based APTSCs in terms of Voc, short-circuit current density (Jsc), fill factor (FF), and power conversion efficiency (PCE).

The ETL material alternatives were titanium dioxide (TiO_2), tin (IV) oxide (SnO_2), zinc oxide (ZnO) and phenyl-C71-butyric acid methyl ester (PCBM), whereas HTL material options include copper (I) oxide (Cu_2O), 2,2',7,7'-Tetrakis (N,N-di-p-methoxyphenylamine) 9,9'- spirobifluorene (Spiro-OMeTAD), poly (3,4-ethyelenedioxythiophene) polysterene sulfonate (PEDOT:PSS) and poly (3-hexythiophene) (P_3HT). The ETL was manipulated with four different materials, while HTL remained as Spiro-OMeTAD. The contact, perovskite, and other layers are kept constant throughout the simulation. Repeating these procedures for HTL simulation, PCBM was employed as the material for the ETL.

3. RESULTS AND DISCUSSION

3.1 Optimum Layer Thickness

The results of the photovoltaic parameter that include PCE, Jsc, Voc and FF against Ge and SnGe-perovskite layer thicknesses are as illustrated in Figure 2. It is proved that by varying the layer thickness, the overall solar cell efficiency may be improved. At a thickness between 100 m and 400 nm for Ge-perovskite layer, the PCE increased exponentially from 2.88% to 4.66%, then with a slight drop to 4.46% subsequently at 500 nm. From the fluctuating pattern for SnGe-perovskite layer thickness, the second highest PCE happened at 100 nm and 500nm respectively with 5.42%, while the peak PCE was 6.52% at 300 nm. The device structure also yielded Voc of values ranging from 0.969 V and 0.994 V for both Ge and SnGe-perovskite layer thicknesses simulations differing from 100 nm to 500 nm. The Voc trend of this Ge/SnGe perovskite design declined alongside with the perovskite layer thicknesses.

Furthermore, for the Jsc of Ge-based perovskite, an increasing trend was obtained. As the thickness of Ge-perovskite rose from 100 nm to 500 nm, the Jsc increased by 2.0 mA/cm^2 from 3.4 mA/cm^2 to 5.4 mA/cm^2. The pattern of SnGe-perovskite layer's curve turned out as a fluctuating trend. The Jsc started from 6.3 mA/cm^2 and went down to 4.4 mA/cm^2, followed by a 3.3 mA/cm^2 increased (4.4 mA/cm^2 to 7.7 mA/cm^2) at 300 nm, dropped to 5.6 mA/cm^2 (at 400 nm) and finally increased back to 6.5 mA/cm^2 at 500 nm. Based on Figure 2(d), both the results for FF of the layer thickness variations displayed curves of decreasing trends. It showed that at

maximum performance efficiency (4.66%), the FF was at the lowest (0.845) of all other variation ranges for Ge-perovskite layer thickness. The FF started from 0.863 (100 nm), which subsequently decreased to 0.851 as the layer thickness increased to 400 nm.

It was reported that as the thickness of the single-junction absorber layer, $CsSnGeI_3$ increases, the PCE showed a hiking followed by stable trend, where the maximum PCE that was achieved by the SnGe-perovskite was as high as approximately 31% [23]. Based on previous studies, as the metal work function of both $MAGeI_3$ and $CsSnGeI_3$ perovskite layers increased, the Voc, FF and PCE demonstrated increasing trends, then were saturated. This proved that optimized work function of metal helps enhance the overall efficiency correspondingly, which in turn improves the device performance [22].

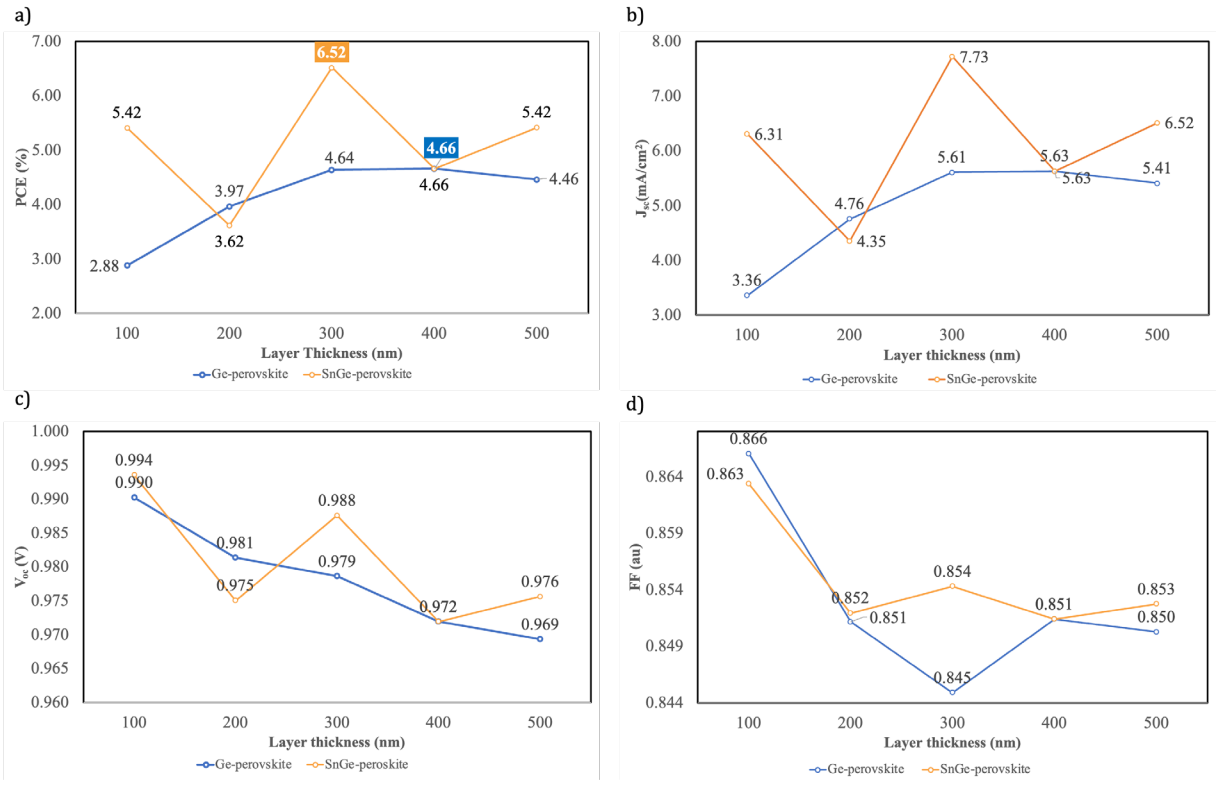

Figure 2. Influence of layer thickness on (a) power conversion efficiency (PCE) (b) open-circuit voltage (Jsc) (c) short-circuits current density (Voc) (d) fill factor (FF).

The resulting parameters of optimum layer thicknesses Ge and SnGe-based all-perovskite tandem solar cells are listed in Table 1. The highest PCE occurred at optimum thicknesses of 400 nm and 300 nm for $MAGeI_3$ and $FAMASnGeI_3$ respectively. According to Singh *et al*. [17], when SnGe-perovskite is 300 nm thick, the PCE peaks at 22.3%, while Ge-perovskite best performs at 200 nm thickness. Power conversion efficiency increases as layer thickness increases. The optimum thickness of SnGe-perovskite in this study indicated similar thickness; however, Ge-perovskite was slightly higher (400 nm) due to software limitations. The total perovskite thicknesses for both studies were within 1000 nm.

Table 1 Output of maximum performance with optimum Ge and SnGe-perovskite thicknesses

Output Parameter			Resulting Value
Active Layer Thickness (nm)	WBG Perovskite	$MAGeI_3$	400
	HTL	Spiro-OMeTAD	350
	ETL	PCBM	70
	NBG Perovskite	$FAMASnGeI_3$	300
Bandgap (eV)	WBG Perovskite	$MAGeI_3$	1.8
	NBG Perovskite	$FAMASnGeI_3$	1.4
PCE (%)			6.52
V_{oc} (V)			0.988
J_{sc} (mA/cm^2)			7.7
FF			0.854

3.2 Optimum Bandgap Layer

The outcome of PCE, Voc, Jsc and FF of Ge and SnGe perovskites with corresponding layer bandgap values are displayed in Figure 3 and Figure 4. Based on Figure 3(a), when the bandgap of Ge-perovskite layer was first manipulated, the PCE hiked up dramatically as the bandgap surged. The PCE expressed an increasing trend from 6.3% at 1.5 eV, to 7.8% at 1.8 eV. From 1.8 eV bandgap onwards, the PCE of the Ge/SnGe perovskite device hovered at 7.8%. Consequently, after applying the optimum bandgap of 1.8 eV for Ge-perovskite, as the SnGe-perovskite bandgap increased, the PCE demonstrated an overall increasing graph pattern. Based on Figure 4(a), despite the minor decrement from 3.8% (1.0 eV) to 1.6% at 1.1 eV at the early stage, the PCE rose exponentially from that onwards to 6.3% at 1.4 eV.

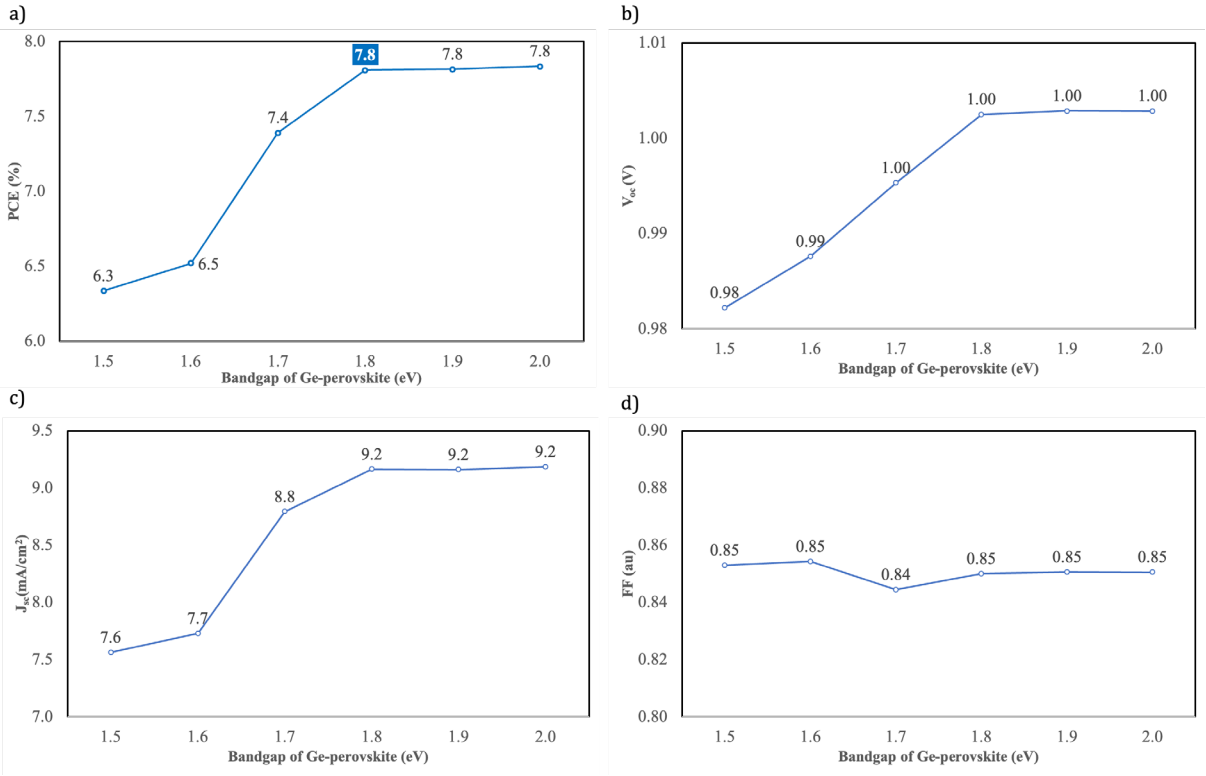

Figure 3. Influence of bandgap on (a) power conversion efficiency (b) open-circuit voltage (c) short-circuits current density (d) fill factor of Ge-perovskite.

For wide bandgap, Ge-perovskite bandgap variation, the Voc rose marginally from 0.98 V to 1.00 V, at 1.5 eV and 1.7 eV bandgaps respectively based on Figure 3(b). After 1.7 eV Ge-perovskite bandgap, the Voc remained constant at 1.00 V even at 2.0 eV Ge-perovskite bandgap. With the optimum Ge-perovskite bandgap of 1.8 eV, the pattern of the Voc of SnGe-perovskite displayed an overall increasing trend. In Figure 4(b), the optimal Voc value is at 1.00 V for Ge-perovskite and 0.82 V for SnGe-perovskite, at optimum bandgaps of 1.8 eV and 1.4 eV respectively, were obtained.

Next, for Jsc, both variations of Ge and SnGe-perovskite bandgap yielded gradually decreasing trends as shown in Figure 3(c) and Figure 4(c). As the Ge-perovskite bandgap escalated from 1.5 eV to 1.8 eV, there was a steep plunge in Jsc from 76 A/m^2 to 92 A/m^2. After that, it remained consistent even when Ge-perovskite bandgap soared to 2.0 eV. For SnGe-perovskite, there was at first a sharp decrease of Jsc from 6.6 mA/cm^2 to 2.0 mA/cm^2 at 1.0 eV and 1.1 eV bandgap correspondingly, before the overall increasing trend occurred. From 1.1 eV bandgap onwards, the Jsc increase from the initial 2.0 mA/cm^2 to 9.2 mA/cm^2 at 1.4 eV. the highest FF of WBG and NBG perovskite layer bandgaps were 0.85 and 0.86 respectively. Overall, the pattern of the FF curves indicated a considerably uninterrupted trend plotted in Figure 3(d) and Figure 4(d). The highest FF of Ge and SnGe-perovskite layer bandgaps were 0.85 and 0.86 respectively.

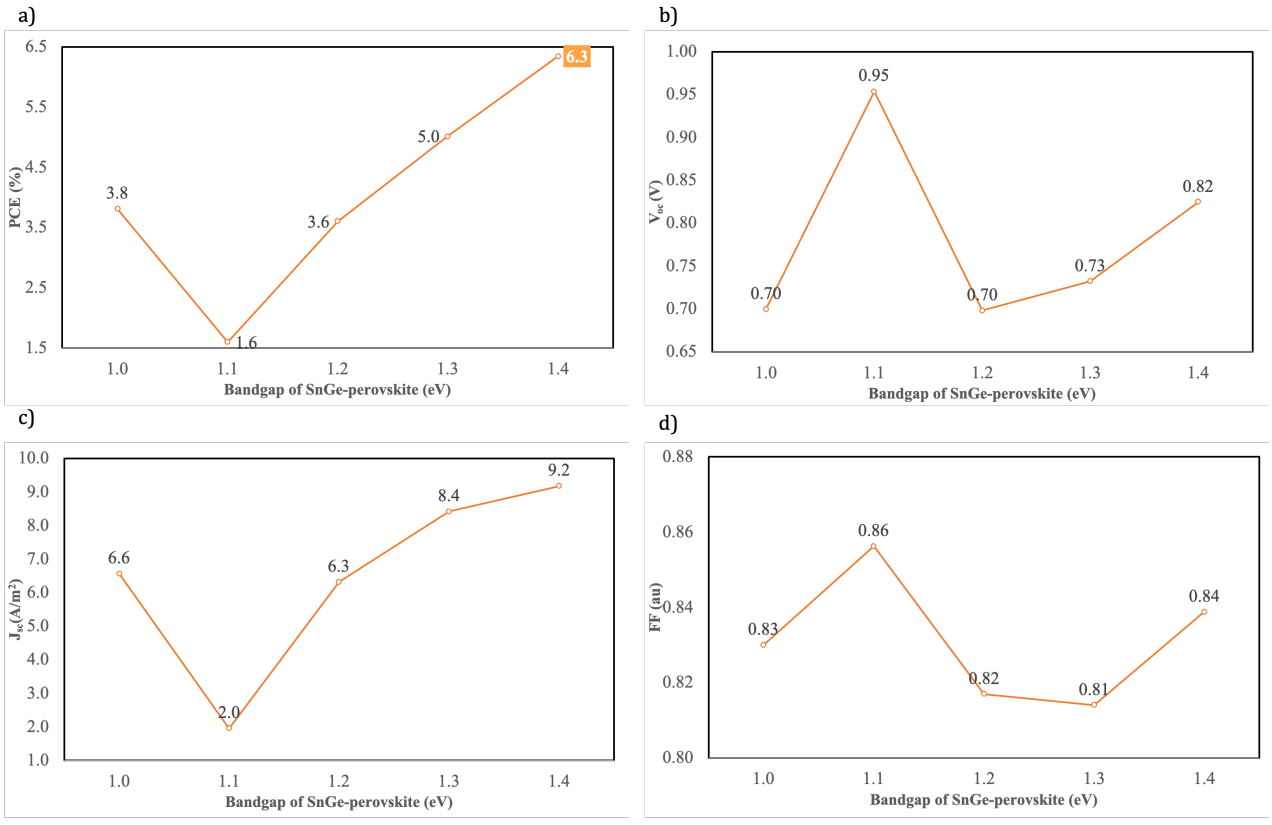

Figure 4. Influence of bandgap on (a) power conversion efficiency (b) open-circuit voltage (c) short-circuits current density (d) fill factor of SnGe-perovskite.

According to Zheng [21], the combination of $FAMASnGeI_3$ of 1.4 eV and $MAGeI_3$ of 1.9 eV yielded a gradually increasing PCE up to 26.72%. Despite the PCE being lower due to several limitations, the output of this research is acceptable since the optimum bandgaps of Ge and SnGe perovskites at maximum PCE were very close to that of previous studies. The basic concept of the impact of perovskite layer bandgap towards the Voc is that when the bandgap increases, the Voc increases. The dominating effect of the increasing Voc determines the rise or drop of the overall PCE. In

comparison with this concept, the result of this study is in line with the previous study since the resulting Voc shot up as the bandgaps of Ge and SnGe-perovskite layers went up [18].

The bandgap of the material plays a significant role in affecting the output value of Jsc of a solar cell. The reason is that as the layer bandgap inclines, it allows additional absorption of photons of small energy, which as a result increases the short-circuit current [24]. Since the short-circuit current is inversely proportional to the Jsc, the outcomes of the variation of Ge and SnGe-perovskite bandgaps is accurate as it abides to this concept. With that, this proved that the Jsc has direct influence on the rise or fall of the overall performance efficiency of solar cells.

Table 2 displays output of Ge/SnGe-perovskite at optimum bandgaps. In continuation of thickness simulation, the optimum bandgaps of Ge and SnGe-based perovskite were utilized. The greatest PCE was performed at optimum Ge-perovskite (WBG) bandgap of 1.8 eV (7.8%) initially, following SnGe-perovskite (NBG) bandgap of 1.4 eV at 6.3% PCE. As bandgap increased, PCE and Voc showed similar trend due to dominating combined effect, while Jsc dipped as photon energy absorption was reduced. These results follow the concept of Voc indirectly proportional to Jsc [25].

Table 2 Output of maximum performance with optimum Ge and SnGe-perovskite bandgaps

Output Parameter			**Resulting Value**
Active Layer Thickness (nm)	WBG Perovskite	$MAGeI_3$	400
	HTL	Spiro-OMeTAD	350
	ETL	PCBM	70
	NBG Perovskite	$FAMASnGeI_3$	400
Bandgap (eV)	WBG Perovskite	$MAGeI_3$	1.8
	NBG Perovskite	$FAMASnGeI_3$	1.4
PCE (%)			6.35
V_{oc} (V)			0.82
J_{sc} (mA/cm^2)			9.2
FF			0.84

3.3 Best Performing ETL-HTL Material

Table 3 shows how the photovoltaic performance is influenced by different ETL and HTL materials. When PCBM was used as the ETL material, the optimal PCE of 6.35% was achieved, as the Voc and FF peaked at 0.825 V and 0.839 respectively, while Jsc was at its highest 9.2 A/m2. This was due to reduction in charge transportation resistance and increase in recombination resistance. The PCE significantly increased from 2.64% (ZnO) to 6.35% (PCBM). The best performing ETL for $CsSnGeI_3$ was SnO_2 with 30.9% PCE, followed by TiO_2 [23]. Despite differences in PCE, this study showed same trend as SnO_2 and TiO_2 are the second and third best performing of all ETL materials. For $MASnI_3$, PCBM peaked in PCE and was chosen as the final ETL material [26].

For HTL simulation, when HTL material was PEDOT: PSS, it showed the highest PCE (11.12%) which shot up by 3.05% after P_3HT. The Voc and Jsc when HTL was PEDOT: PSS also surged to 0.840 V and 16.1 mA/cm^2 respectively, while the FF shrank to 0.825%. Previous studies stated that the best performing HTL material was Cu2O [26], which this current study contradicts as photovoltaic performances are greatly influenced by material fabrication criteria. Singh [22] deduced that Cu_2O had the highest PCE (18.01%), while PEDOT: PSS was second best performing. The application of secondary data, difference in ETL and HTL thicknesses via the One-

Dimensional Solar Cell Capacitance Simulator (SCAPS-1D) were the main causes of differences. Nevertheless, PEDOT: PSS was one of the most efficient HTL material for both studies, so this result is acceptable. In short, the most suitable ETL-HTL combination is PEDOT-PCBM.

Table 3 Output of best performing ETL-HTL material combinations

ETL-HTL Combination	V_{oc} (V)	J_{sc} (mA/cm^2)	FF	PCE (%)
ETL Simulation (HTL: Spiro-OMeTAD)				
TiO_2	0.804	4.3	0.829	2.85
SnO_2	0.805	4.4	0.830	2.97
ZnO	0.803	4.0	0.826	2.64
PCBM	0.825	9.2	0.839	6.35
HTL Simulation (ETL: PCBM)				
Spiro-OMeTAD	0.825	9.2	0.839	6.35
PEDOT: PSS	0.840	16.1	0.825	11.12
p3HT	0.830	12.0	0.810	8.07
Cu_2O	0.820	7.0	0.850	4.90

Figure 5 presents current density-velocity (J-V) curve of the best performing ETL-HTL combination. Spiro-PCBM combination was the original structure (Figure 1), however, PEDOT-PCBM is the final structure and best performing all-perovskite tandem solar cell design in this study. This graph was obtained using the optimum layer thicknesses for Ge and SnGe-perovskites at 400 nm and 300 nm correspondingly. Ge (1.8 eV) and SnGe-perovskites (1.4 eV) were also at their optimum bandgaps.

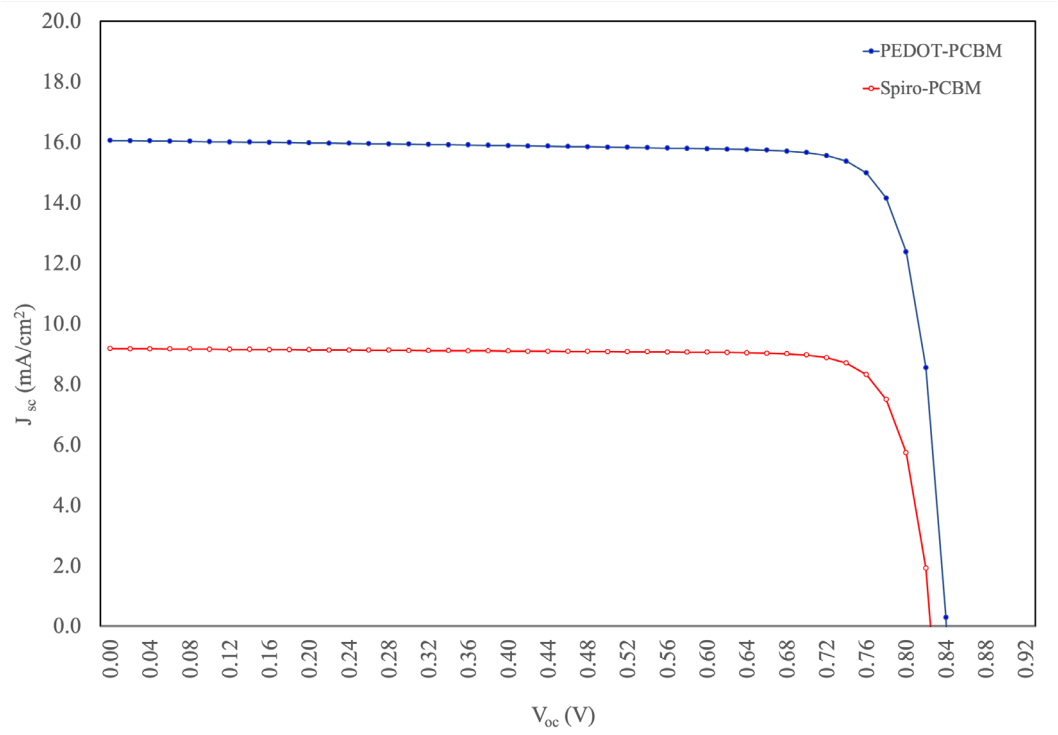

Figure 5. J-V curves of highest PCE (PEDOT-PCBM) and original structure (Spiro-PCBM).

It was observed that the Jsc of Spiro-PCBM combination was consistently higher than that of PEDOT-PCBM when Voc was 0 V to 0.88 V. After that, from 0.88 V to 0.92 V, the steepness of both the J-V curves were nearly identical to each other. This outcome was appropriate because Voc is inversely proportional to Jsc. Since the PEDOT-PCBM combination yielded a lower overall Jsc than that of Spiro-PCBM, it performed better than the Spiro-PCBM combination. This statement is accurate as PCE of Spiro-PCBM is only 6.35%, while PEDOT-PCBM is higher, at 11.12%.

5. CONCLUSION

The problems stated in this study were that the traditional silicon-based solar cells are costly and solid-structured (requires huge storage space), and lead-based PSCs (water soluble) cause catastrophic effects upon consumption. The design of the lead free all-perovskite tandem solar cell was therefore proposed as a solution. The optimum layer thickness of Ge and SnGe-perovskite were 400 nm and 300 nm respectively, which total thickness equalled 700 nm. In addition, the combination of PCBM (ETL) and PEDOT:PSS (HTL) showed maximum PCE of 11.12% (Voc = 0.84 V, Jsc = 16.1 mA/cm^2, FF = 0.825). Hence, the design with PEDOT-PCBM was the best performing ETL-HTL combination.

In this study, the $FAMASnGeI_3$ and $MAGeI_3$ were chosen as the NBG and WBG materials respectively as it is considered low cost due to the ability of using solution-based fabrication. Since the study focuses on the optimization of the thickness of the perovskite absorber layer and the selection of ETL and HTL materials in the tandem structure, other parameters such as the thickness variation of the ETL and HTL materials, bandgap variations, electron and hole mobility and defect density are held constant for ease of applications. This explains the lower efficiency obtain compared to the other simulated works.

To further improve the efficiency of the simulated work, several strategies can be employed which include bandgap optimization of the NBG and WBG materials, that can be done by modification of the A-site and B-site cations. The optimization of bandgap will enable maximum absorption of light while reducing the losses in Voc. Besides that, modification of the interface between the ETL/perovskite layer is vital in obtaining a higher efficiency by enhancing the electron extraction while reducing recombination and defect passivation.

While PEDOT:PCBM shows the best performing ETL-HTL combination, other ETL/HTL combination should also be studied which include indium–gallium–zinc–oxide (IGZO), tungsten disulfide (WS2), C60, ceric dioxide (CeO_2) as the ETL and Copper(I) thiocyanate (CuSCN), nickel oxide (NiO), CFTS and CBTS as the HTL. In addition, optimization on the thickness of the ETL and HTL can also leads to better performance of the PSCs. Furthermore, recent study also shows that in addition to the dual junction tandem structure, a triple junction tandem structure is also possible to further increase the overall efficiency of the PSCs. To conclude, this research may contribute to future research on the all-perovskite tandem solar cell field where the accuracy of PEDOT-PCBM performance can be further studied.

ACKNOWLEDGEMENT

The authors would like to acknowledge the support from the Fundamental Research Grant Scheme under grant number FRGS/1/2021/TK0/UNIMAP/02/49 from the Ministry of Education Malaysia. The authors are thankful to Dr. Roderick Mackenzie (Assistant Professor in the Department of Engineering of the Durham University of Gent, United Kingdom) for providing OghmaNano (GVPDM) software.

REFERENCES

[1] Soga, T., Chapter 1 - Fundamentals of Solar Cell, in Nanostructured Materials for Solar Energy Conversion, T. Soga ed. Elsevier: Amsterdam 2006 pp. 3-43.
[2] Muhammad Aamir, I., *et al*., Materials for Photovoltaics: Overview, Generations, Recent Advancements and Future Prospects, in Thin Films Photovoltaics, Z. Beddiaf and S. Chander ed. Intech Open: Rijeka 2022 pp. Ch. 2.
[3] Mohammad Bagher, A., American Journal of Optics and Photonics, vol 3, issue 5 (2015).
[4] Anshebo Getachew, A. & A. Teketel, Recent Development of Lead-Free Perovskite Solar Cells, in Recent Advances in Multifunctional Perovskite Materials, S. Poorva and K. Ashwini ed. Intech Open: Rijeka 2022 pp. Ch. 7.
[5] Li, J., *et al*., Nano Energy, vol 80, issue 2021) pp. 105526.
[6] Wang, M., *et al*., Nano-Micro Letters, vol 13, issue 1 (2021) pp. 62.
[7] Azhari, A. W., *et al*. "Tin and germanium substitution in lead free perovskite solar cell: Current status and future trends". in IOP Conference Series: Materials Science and Engineering.
[8] Jiang, X., *et al*., ACS Photonics, vol 10, issue 6 (2023) pp. 1992-1998.
[9] Li, H. & W. Zhang, Chemical Reviews, vol 120, issue 18 (2020) pp. 9835-9950.
[10] Oladapo, S., B. M. Soucase, & B. Aka, IOSR Journal of Applied Physics, vol 08, issue 04 (2016) pp. 01-11.
[11] Eperon, G. E., M. T. Hörantner, & H. J. Snaith, Nature Reviews Chemistry, vol 1, issue 12 (2017) pp. 0095.
[12] Jiang, F., *et al*., Journal of Materials Chemistry A, vol 4, issue 4 (2016) pp. 1208-1213.
[13] Palmstrom, A. F., *et al*., Joule, vol 3, issue 9 (2019) pp. 2193-2204.
[14] Lin, R., *et al*., Nature Energy, vol 4, issue 10 (2019) pp. 864-873.
[15] Lin, R., *et al*., Nature, vol 620, issue 7976 (2023) pp. 994-1000.
[16] Madan, J., *et al*., Solar Energy, vol 197, issue 2020) pp. 212-221.
[17] Singh, N., A. Agarwal, & M. Agarwal, Solar Energy, vol 208, issue 2020) pp. 399-410.
[18] Abdelaziz, S., *et al*., Optical Materials, vol 123, issue 2022) pp. 111893.
[19] Duha, A. U. & M. F. Borunda, Optical Materials, vol 123, issue 2022) pp. 111891.
[20] Filip, M. R. & F. Giustino, The Journal of Physical Chemistry C, vol 120, issue 1 (2016) pp. 166-173.
[21] Zheng, X., &., Accounts of Materials Research, vol 1, issue 1 (2020) pp. 63-76.
[22] Singh, N., A. Agarwal, & M. Agarwal, Superlattices and Microstructures, vol 149, issue 2021) pp. 106750.
[23] Sabbah, H. Numerical Simulation of 30% Efficient Lead-Free Perovskite CsSnGeI3-Based Solar Cells. Materials, 2022. 15, DOI: 10.3390/ma15093229.
[24] Morales-Acevedo, A., Solar Energy, vol 83, issue 9 (2009) pp. 1466-1471.
[25] Zouhair, S., *et al*., Solar RRL, vol 6, issue 2 (2022) pp. 2100745.
[26] Sarker, S., I., Materials Today Communications, vol 32, issue 2022) pp. 103881.